NASA TECHNICAL MEMORANDUM

NASA TM X-3121

NASA TM X-3121

FLIGHT REYNOLDS NUMBER EFFECTS ON A FIGHTER-TYPE, CIRCULAR-ARC - 19° CONIC BOATTAIL NOZZLE AT SUBSONIC SPEEDS

by Roger Chamberlin

Lewis Research Center
Cleveland, Ohio 44135

NATIONAL AERONAUTICS AND SPACE ADMINISTRATION • WASHINGTON, D. C. • OCTOBER 1974

FLIGHT REYNOLDS NUMBER EFFECTS ON A FIGHTER-TYPE, CIRCULAR-ARC - 19° CONIC BOATTAIL NOZZLE AT SUBSONIC SPEEDS

by Roger Chamberlin

Lewis Research Center

SUMMARY

A circular-arc - conic boattail nozzle, typical of those used on a twin engine fighter, was tested on an underwing nacelle mounted on an F-106B aircraft. The boattail had a radius ratio r/r_c of 0.41 and a terminal boattail angle of approximately 19°. The gas generator was a J85-GE-13 turbojet engine. The effects of Reynolds number and angle of attack on boattail pressure drag and boattail pressure profiles were investigated.

Increasing Reynolds number resulted in reduced boattail drag at both Mach numbers of 0.6 and 0.9. The sensitivity of boattail drag to Reynolds number on this nozzle was greater than that of a 16° boattail, but less than that of a 24° boattail. The change in drag was associated with a change in the extent of the separated region over the Reynolds number range. This was verified analytically by moving an assumed separation point upstream to duplicate the changes seen in the pressure profiles between high and low Reynolds numbers.

INTRODUCTION

The Lewis Research Center is conducting a flight and wind tunnel program investigating the effects of Reynolds number on exhaust nozzle performance. The majority of testing at this time has been concerned with nozzle pressure drag. A series of high angle boattail nozzles have been tested (refs. 1 to 4). These nozzles are designed for operation behind a turbofan engine on an aircraft that cruises subsonically, but has supersonic dash capability. In the flight range of Reynolds numbers these boattails all have shown a reduction in boattail drag with increasing Reynolds number. Some of the geometries experienced only a small effect, while for others the change

in drag was considerable. This was the result of increased compression of the flow on the aft boattail at higher Reynolds numbers. The cause of the phenomenon appeared to be a decrease in the amount of separated flow on the aft boattail surface.

The flight investigation herein concerns one of these high angle boattail nozzles, typical of that used on a twin engine fighter. The nozzle was fixed with the boattail in the closed or subsonic cruise configuration. The purpose of this study was to determine the effect of Reynolds number on the boattail drag and pressure distribution of this particular geometry. The geometry was a combination circular arc transitioning into a double conic section. The circular-arc portion had a radius ratio r/r_c of 0.41. This transitioned into a 19.5° conic section, which then reduced to an 18.2° conic section on the end of the boattail.

The flight tests were conducted with the boattail mounted on a nacelle under the wing of a modified F-106B aircraft (fig. 1) (refs. 5 to 8). The exhaust nozzle is located just downstream of the wing trailing edge. Data were taken at altitudes from 4572 to 13 716 meters (15 000 to 45 000 ft) yielding nominal Reynolds number variations at the boattail between 71.0×10^6 and 23.1×10^6. Data were recorded at Mach numbers of 0.6 and 0.9, and angle of attack was varied from 4.6° to 9.1°.

SYMBOLS

A	area
A_{E8}	nozzle effective throat area (hot), cm^2 (sq in.)
A_e	nozzle exit area, 771.59 cm^2 (119.60 sq in.)
A_{max}	maximum cross-sectional area, 3167.12 cm^2 (490.87 sq in.)
C_D	drag coefficient, D/q_0A_{max}
C_p	pressure coefficient, $(p - p_0)/q_0$
D	pressure drag, N (lb)
d	maximum nacelle diameter, 63.50 cm (25.00 in.)
h	altitude, m (ft)
L	characteristic length, 5.18 m (17.00 ft)
l	nozzle length, 62.74 cm (24.70 in.)
M	Mach number
P	total pressure, N/m^2 abs (psia)
p	static pressure, N/m^2 abs (psia)

q dynamic pressure, N/m^2 abs (psia)

Re Reynolds number, $\rho vL/\mu$

r radius of boattail shoulder, cm (in.)

r_c radius of a full circular-arc boattail making the same area transition as the boattail of this report, cm (in.)

T total temperature, K (^oR)

v velocity, m/sec (ft/sec)

x axial distance from boattail shoulder nacelle station 530.63 cm (208.91 in.)

y radial distance from nozzle centerline to boattail surface, cm (in.)

α angle of attack, deg

μ coefficient of viscosity, $N\text{-sec}/m^2$ (slug/ft-sec)

ρ density, kg/m^3 (slug/cu ft)

Subscripts:

0 free stream

8 primary nozzle throat station

APPARATUS AND PROCEDURE

Installation

Details of the airplane modifications and the nacelle-engine assembly are given in references 6 and 7. A schematic and a photograph of the nacelle and boattail nozzle are shown in figures 2 and 3. The nacelle was located at the 32 percent semispan and alined parallel to the aircraft centerline. The nacelle had a downward incidence of $4\frac{1}{2}^o$ (relative to the wing chord) so that the aft portion of the nacelle was tangent to the aft wing lower surface, and provided approximately 0.64-centimeter (0.25-in.) clearance at the wing trailing edge. Details of the wing modifications, nacelle shape, and mounting strut are given in reference 7. The strut with the wide fairing described in reference 7 was used.

The gas generator for this nozzle was a J85-GE-13 turbojet engine with afterburner. The variable area primary nozzle was locked at 709.70 square centimeters (110 $in.^2$) permitting operation at military or part power. The secondary cooling airflow was controlled by a rotary valve just ahead of the compressor face (fig. 2).

Because the ratio of the nozzle exit area to primary area was small ($A_e/A_8 = 1.09$), this nozzle could pump only small amounts of secondary air (approx. 1 percent of the primary flow); so the secondary flow valve was fixed in the full-open position. The load cell was not operational for this series of tests.

Test Hardware

A photograph of the boattail installed on the aircraft is shown in figure 4. The dimensions of the nozzle and boattail are shown in figure 5. The circular arc portion of the boattail had a radius ratio of 0.41. The radius ratio is defined as r/r_c where r is the actual radius of the boattail and r_c is the radius of a complete circular-arc boattail making the same area transition and terminating with the same 19^o angle. The ratio of nozzle exit area to nacelle area was $A_e/A_{max} = 0.24$. A more detailed representation of the geometry is given in figure 5. A nickel-chromium-base alloy (Rolled Alloy 333) was used for the internal portions of the nozzle, and the external parts were predominately 304 stainless steel.

Instrumentation

An onboard data recording system was developed specifically for the F-106 program (ref. 8), and as a result it was possible to instrument the nozzle quite extensively (see fig. 6). The nozzle had 12 rows of static pressure orifices equally spaced circumferentially around the boattail. There were nine ports in each row spanning the length of the boattail and all 108 pressures were area weighted to simplify the boattail drag calculations. Four nonarea weighted static pressure taps were located near the boattail shoulder and nine more on the cylindrical section upstream of the boattail.

Tufts were mounted on the upper quadrant of the boattail, and pictures of the tufts were taken with a high-speed motion picture camera mounted in the tail (see ref. 1). The camera was integrated with the data system so that it ran only during each of the 11.60-second data scan periods.

Data Reduction

Engine airflow was determined using prior engine calibration data (ref. 9) along with inflight measurements of engine speed, pressure, and temperature at the compressor face. Knowing the compressor inlet flow, the total pressure and temperature at the turbine discharge, and the fuel flow rates, other parameters at the primary

nozzle exit, such as effective area A_{E8}, total pressure P_8, and total temperature T_8, were obtained from previous calibrations. All the drag values were determined by pressure integration.

Each scanivalve had the capability to sample 48 pressures; thus three scanivalves were required to measure the 108 boattail pressures. A common pressure, the nose boom free stream static was connected to one port on each scanivalve. In order to account for slight differences or shifts in calibrations between transducers, an average was calculated for the nose boom pressure measurements from the scanivalves. Pressures measured by each scanivalve were then adjusted by the difference between the average value and the value measured by that scanivalve providing a zero shift calibration for each of the scanivalves on each data scan.

Procedure

All the flights were made from Selfridge Air National Guard Base in Mt. Clemens, Michigan, in a test corridor over Lake Huron. A total of three flights were made and all of the data were taken at Mach numbers of 0.6 and 0.9. The ranges of flight variables, speed, altitude, angle of attack, and load factor are listed in table I. All of the data were taken in coordinated turns. The means of varying Reynolds number was to change altitude while holding the Mach number constant. By flying in turns, angle of attack as well as Mach number could be held constant. Also at a given altitude and Mach number, angle of attack could be varied by flying tighter turns increasing the load factor. The J85 engine was run at military power for all of the data points yielding nominal nozzle pressure ratios from 2.7 to 3.2 at Mach 0.6, and from 3.8 to 4.2 at Mach 0.9.

RESULTS AND DISCUSSION

Reynolds Number Effects

Previous flight tests of various boattail shapes have shown that pressure drag on high angle circular-arc - conic boattails is sensitive to Reynolds number (refs. 1 and 2). Of the boattails tested previously all had 24° terminal angles with the exception of one 16° boattail. The subject boattail of this report was a circular-arc - conic boattail with a terminal boattail angle of approximately 19°.

The Reynolds number is based on a characteristic length of 5.18 meters (17.00 ft), which takes into consideration the wing chord at this station (approx. 7.32 m (24.00 ft))

and the nacelle length (approx. 3.96 m (13.00 ft)). Tests were run over a range of Reynolds number at both Mach numbers of 0.6 and 0.9. At Mach 0.9 data were taken at two angles of attack. Reynolds number data at the lower angle ($\approx 4.5^{\circ}$) is shown in figure 7. Data are shown from two flights each covering the whole Reynolds number range. The repeatability of the data between flights was very good. The change in drag with Reynolds number is similar to that found on previous boattails. The slope of the curve is less than found for the 24° boattails, but steeper than that for the 16° boattail (see refs. 1 and 2).

Pressure distributions corresponding to three points on the drag curve are presented in figure 8. Pressure distributions for all meridian angles show a drop in pressure on the aft portion of the boattail at lower Reynolds numbers. There is a circumferential variation in pressure around the boattail due to the presence of the wing and the fuselage in this installation. However, the trend of lower pressures on the aft boattail with lower Reynolds number is consistent at all meridian angles. This appears to be the result of an increase in the amount of separated flow. As the Reynolds number is reduced the boundary layer becomes thicker. With the thicker boundary layer the flow near the surface has less energy and cannot traverse an adverse pressure gradient as far. The result is that the flow if attached will separate and if already separated, the separation point will move upstream.

Further indications of increasing separation with decreasing Reynolds number were seen in the tuft movement on the upper quadrant of the boattail. Figure 9 is a schematic showing the relative tuft movement at a high and low Reynolds number. The shaded areas indicate areas swept over by the tufts. A full circle represents a tuft that at times was pointing in the upstream direction, indicating reverse flow. At the lower Reynolds numbers there was an increase in the area over which obvious reverse flow existed and an increase in the activity of almost all of the tufts. The tufts were approximately 0.64-centimeter- (0.25-in.-) diameter nylon parachute cord with the center core removed. They were glued to the surface and stuck out perpendicular to the surface approximately 2.54 centimeters (1.0 in.). Because of this, they did not always accurately represent the flow right at the boattail surface. They do, however, give a good representation of changes in the overall disturbance of the flow.

Figure 10 presents the Reynolds number effects on boattail drag at a higher angle of attack ($\approx 7.5^{\circ}$). At the higher angle of attack the aircraft could fly to higher altitudes, so lower Reynolds numbers were achieved. These data were taken on two flights also, and again where there is overlap between the two, the repeatability is very good.

Figure 11 presents the pressure distributions corresponding to three points on the drag curve. Again, as at the lower angle of attack, there is a loss of compression on the aft boattail at the lower Reynolds numbers, suggesting an increase in separated flow. Figure 12 shows a schematic of the tuft movement at the high and low Reynolds

numbers. There is an increase in reversed flow and the overall movement of the tufts at the lower Reynolds number.

A limited amount of data was also taken at a Mach number of 0.6. The effect of Reynolds number on boattail drag at Mach 0.6 is shown in figure 13. The corresponding pressure profiles are given in figure 14. The same loss of compression on the aft boattail at low Reynolds numbers is seen again. There is possibly a secondary effect also occurring at Mach 0.6. In addition to the drop in compression on the aft boattail, it appears the pressures along the entire row may be slightly lower at the lower Reynolds numbers. Since the Mach numbers were almost identical for these data points, it can be ruled out as a possible cause. Although it will be shown in the next section that there is no effect of angle of attack on boattail drag at Mach 0.9, previous boattails have shown an angle of attack effect at Mach 0.6 at high angles. These data were taken at a nominal angle of 10°. But the higher Reynolds number data were actually at an angle of attack of 9.3°, and the lower Reynolds number data were at an angle of attack of 10.5°. This variation may be the cause of the shifts in the pressure profiles.

Angle of Attack Effects

The effect of angle of attack was investigated at Mach 0.9 only. There was little or no effect of angle of attack on boattail drag at this Mach number (fig. 15). The angles of attack covered were all relatively low, varying from 4.7° to 9.1°. Pressure distributions at three corresponding angles of attack are shown in figure 16 In general the pressures show no change with angle of attack.

Analytical Verification

An analytical study was conducted to see if the hypothesized changes in the separated flow would indeed result in the observed pressure changes. This was done using an axisymmetric potential flow program with a Goethert compressibility correction (ref. 10). A separation point, was assumed, and an equivalent body, beginning at the separation point, was input in place of the actual geometry. The program then calculated the pressures along this surface and on the boattail ahead of the separation point. The location of the separation point and the shape of the equivalent body were then modified so the resulting calculated pressures agreed with the experimental data at similar axial locations. Near perfect agreement with experimental data was achieved by this technique (fig. 17). To obtain this agreement the shapes of the equivalent bodies had to be contoured, but were very nearly conical. Comparison is made with boattail pressures at the 180° meridian angle because airframe flow field effects were

estimated to be smallest at that location. The calculation was made with the separation point at a downstream location corresponding to a high Reynolds number condition, and then moved upstream to correspond with a low Reynolds number point. The two separation points and corresponding equivalent bodies are shown in figure 18. The required variation in separation point and equivalent body shape to obtain agreement verifies that an increase in the extent of the separated flow region can produce the changes in boattail pressures observed in the flight data.

SUMMARY OF RESULTS

A scaled version of a boattail nozzle typical of those used on a twin engine fighter aircraft, was tested installed just below and aft of the wing trailing edge on an F-106B aircraft at Mach numbers of 0.6 and 0.9. The nozzle was fixed in the closed or military power configuration. The effects of Reynolds number and angle of attack on boattail drag were investigated. The following results were obtained:

1. Increasing the Reynolds number, by reducing altitude (changing density and viscosity), resulted in a decrease in boattail drag at both Mach numbers of 0.6 and 0.9.

2. Increasing Reynolds number produced an increase in compression of the flow on the aft boattail, apparently due to a reduction in the amount of separated flow on the aft boattail. Pictures of tufts on the upper quadrant of the boattail and an analytical calculation also indicated this reduction in separation.

3. At Mach 0.9 there was little or no effect of angle of attack on boattail drag.

4. Analytical calculations verify that an increase in the extent of the separated flow region can result in the same boattail pressure changes as observed in the flight data.

Lewis Research Center,
National Aeronautics and Space Administration,
Cleveland, Ohio, August 1, 1974,
501-24.

REFERENCES

1. Chamberlin, Roger: Flight Investigation of 24° Boattail Nozzle Drag at Varying Subsonic Flight Conditions. NASA TM X-2626, 1972.

2. Chamberlin, Roger; and Blaha, Bernard J.: Flight and Wind Tunnel Investigation of the Effects of Reynolds Number on Installed Boattail Drag at Subsonic Speeds. Paper 73-139, AIAA, Jan. 1973.

3. Wilcox, Fred A.: Comparison of Ground and Flight Test Results Using a Modified F 106B Aircraft. Paper 73-1305, AIAA, Nov. 1973.

4. Chamberlin, Roger: Flight Reynolds Number Effects on a Contoured Boattail Nozzle at Subsonic Speeds. NASA TM X-3053, 1974.

5. Wilcox, Fred A.; Samanich, Nick E.; and Blaha, Bernard J.: Flight and Wind Tunnel Investigation of Installation Effects on Supersonic Cruise Exhaust Nozzles at Transonic Speeds. Paper 69-427, AIAA, June, 1969.

6. Crabs, Clifford C.: An Inflight Investigation of Airframe Effects on Propulsion System Performance at Transonic Speeds. Soc. Experimental Test Pilots, Tech. Rev., vol. 9, no. 4, 1969, pp. 51-66.

7. Mikkelson, Daniel C.; and Head, Verlon L.: Flight Investigation of Airframe Installation Effects on a Variable Flap Ejector Nozzle of an Underwing Engine Nacelle at Mach Numbers from 0.5 to 1.3. NASA TM X-2010, 1970.

8. Groth, Harold W.; Samanich, Nick E.; and Blumenthal, Philip Z.: Inflight Thrust Measuring System for Underwing Nacelles Installed On a Modified F-106 Aircraft. NASA TM X-2356, 1971.

9. Antl, Robert J.; and Burley, Richard R.: Steady-State Airflow and Afterburning Performance Characteristics of Four J85-GE-13 Turbojet Engines. NASA TM X-1742, 1969.

10. Hess, J. L.; and Smith, A. M. O.: Calculation of Potential Flow About Arbitrary Bodies. In Progress in Aeronautical Sciences, Vol. 8, D. Küchemann, ed., Pergamon Press, 1967, pp. 1-138.

TABLE I. - FLIGHT TEST VARIABLES

Altitude, h		Flight Mach number, M_0					
m	ft	0.6			0.9		
		Target angle of attack, α, deg	Nominal Reynolds number, Re	Load factor	Target angle of attack, α, deg	Nominal Reynolds number, Re	Load factor
4 572	15 000	10	47.4×10^6	2.0	5	71.0×10^6	2.3
6 096	20 000	10	40.8	1.6	5	60.8	1.9
7 620	25 000	10	34.6	1.3	5, 8	51.9	1.5, 2.6
9 144	30 000	10	28.9	1.1	5, 8	43.9	1.2, 2.1
10 668	35 000	--	----	---	4.7 – 9.1	36.9	1.0 – 1.9
12 192	40 000	--	----	---	8	29.4	1.3
13 716	45 000	--	----	---	8	23.1	1.0

C-69-2871

Figure 1. - Modified F-106B in flight.

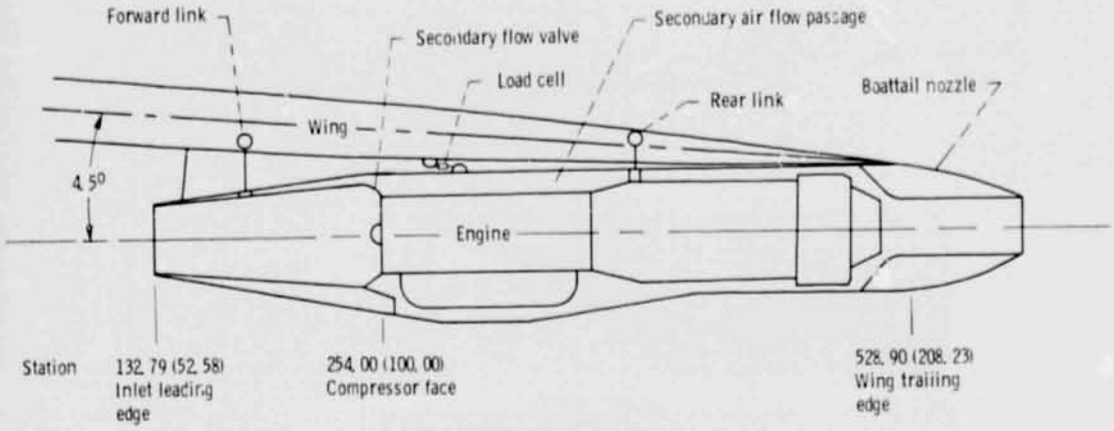

Figure 2. - Schematic of nozzle installation. (All dimensions are in cm (in.) unless indicated otherwise.)

Figure 3. - Nacelle installation on F-106 aircraft.

Figure 4. - Boattail nozzle 4119; radius ratio, 0.41; boattail angle, 19°.

Axial distance from boattail shoulder nacelle station 530.63 cm (208.91 in.), x		Radial distance from nozzle centerline to boattail surface, y	
cm	in.	cm	in.
0.00	0.00	31.75	12.50
6.38	2.51	31.55	12.42
34.65	13.64	25.25	9.94
44.32	17.45	20.82	8.59
62.74	24.70	15.95	6.28

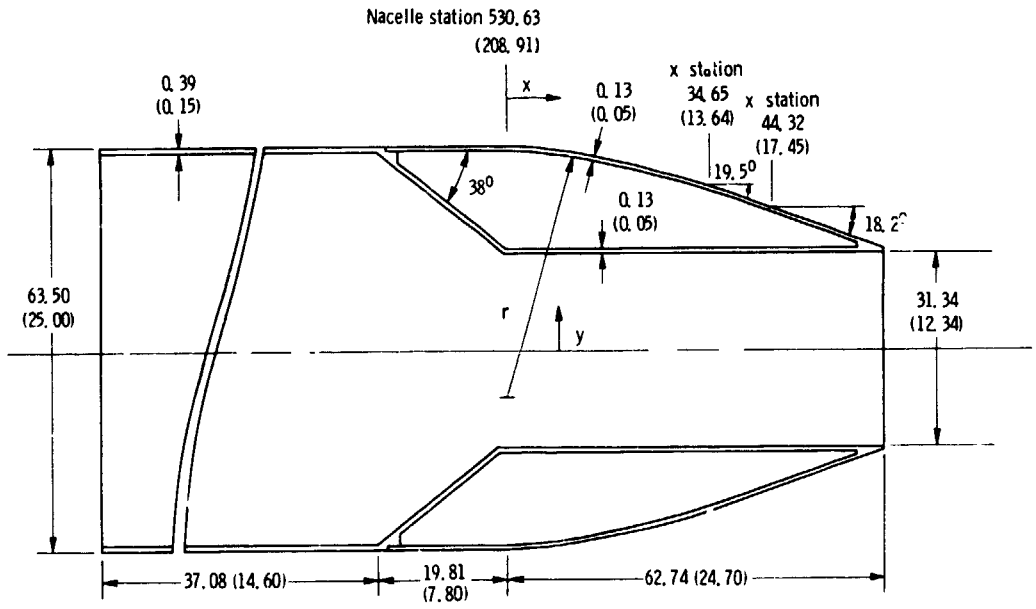

Figure 5. - Boattail nozzle dimensions. Radius of boattail shoulder r = 118.26 (46.56) between x stations 6.38 (2.51) and 34.65 (13.64). (All dimensions are in cm (in.) unless indicated otherwise.)

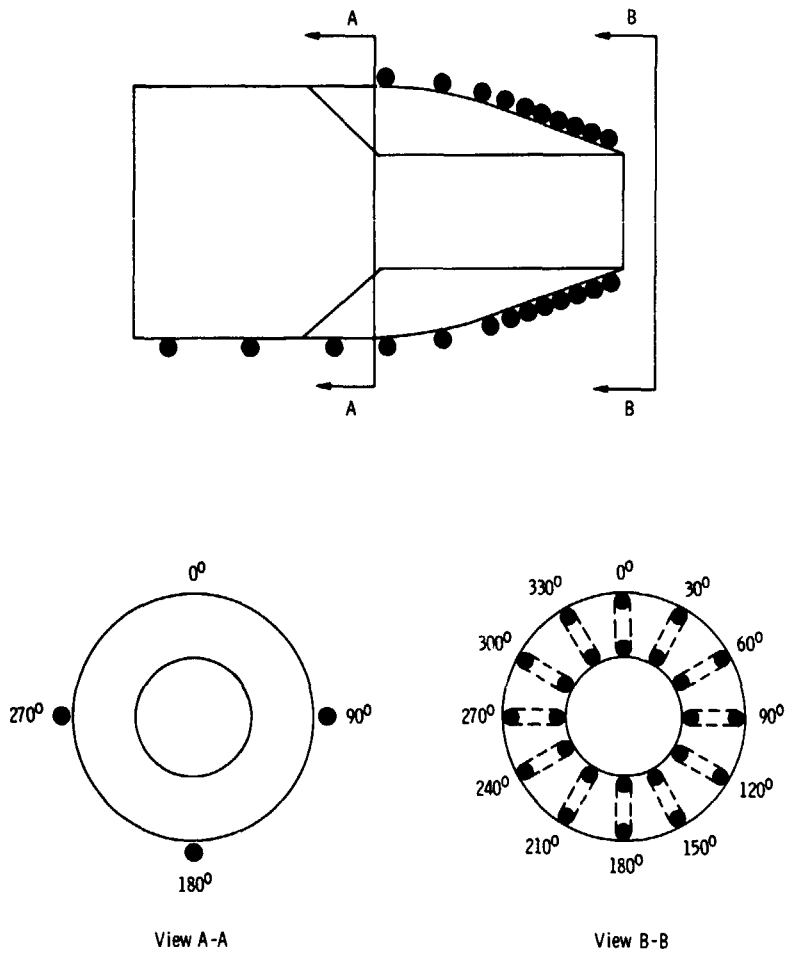

Figure 6. - Boattail nozzle static pressure instrumentation.

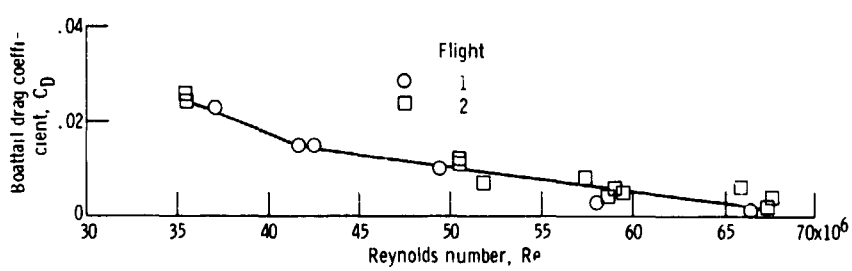

Figure 7. - Reynolds number effect on boattail drag coefficient. Mach number, 0.9; angle of attack, 4.5°.

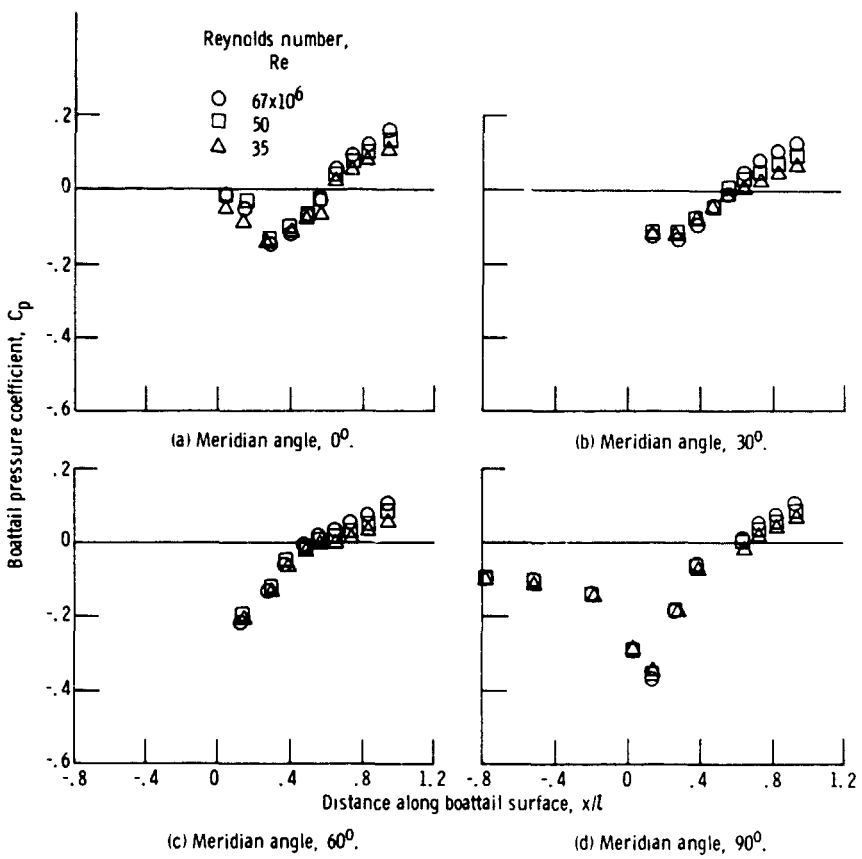

Figure 8. - Effect of Reynolds number on boattail pressure distribution. Mach number, 0.9; angle of attack, 4.5°.

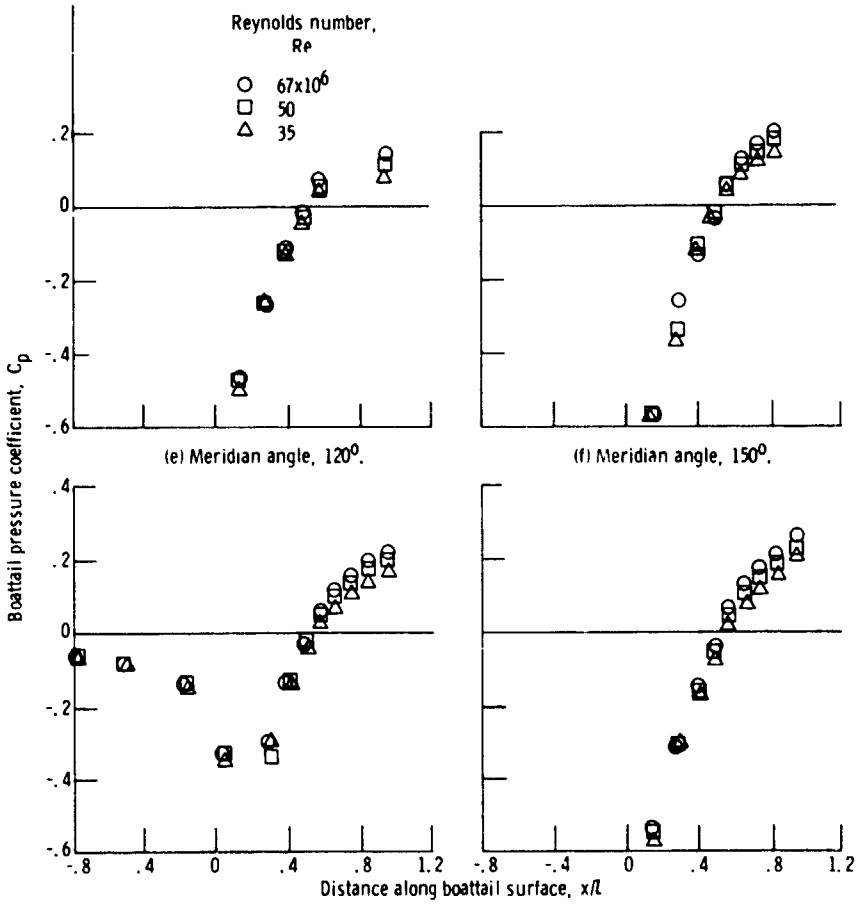

Figure 8. - Continued.

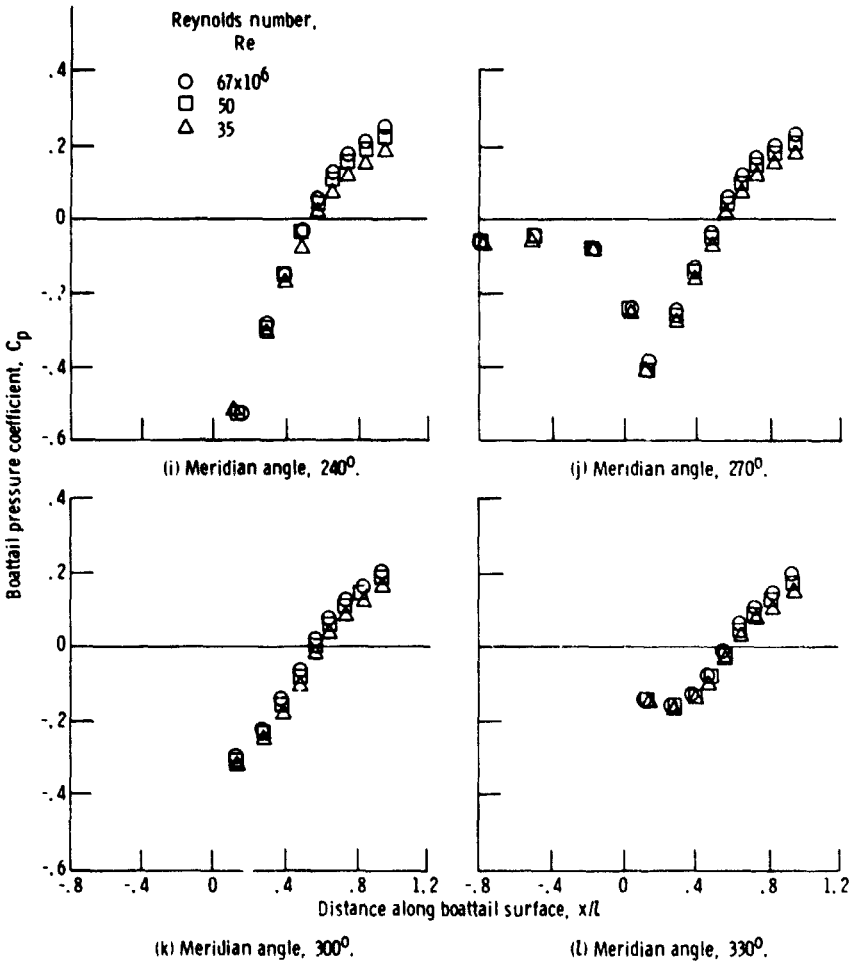

Figure 8. - Concluded.

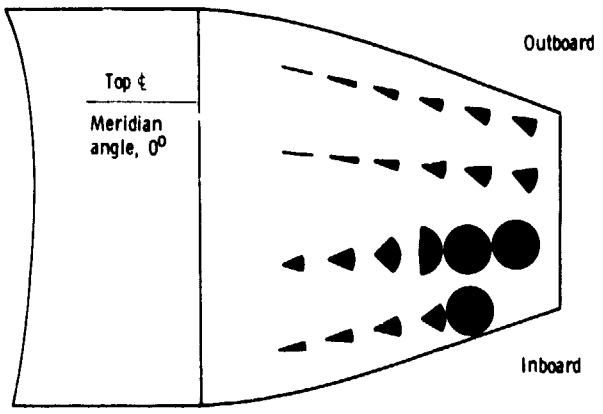

(a) Reynolds number, 50.5x10^6.

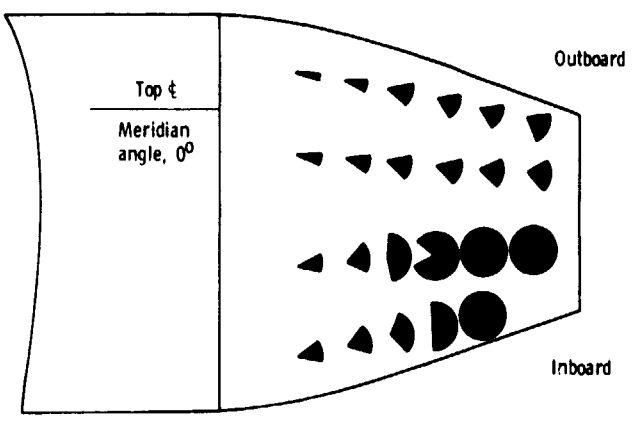

(b) Reynolds number, 35.5x10^6.

Figure 9. - Effect of Reynolds number on amount of tuft movement. Mach number, 0.9; angle of attack, 4.5°. (Shaded areas are areas swept by tuft.)

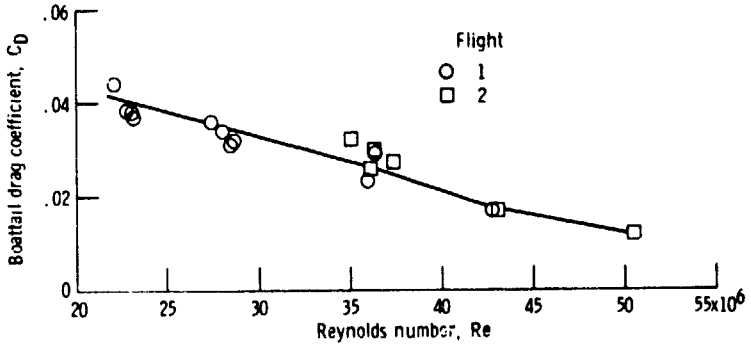

Figure 10. - Reynolds number effect on boattail drag coefficient. Mach number, 0.9; angle of attack, 7.5°.

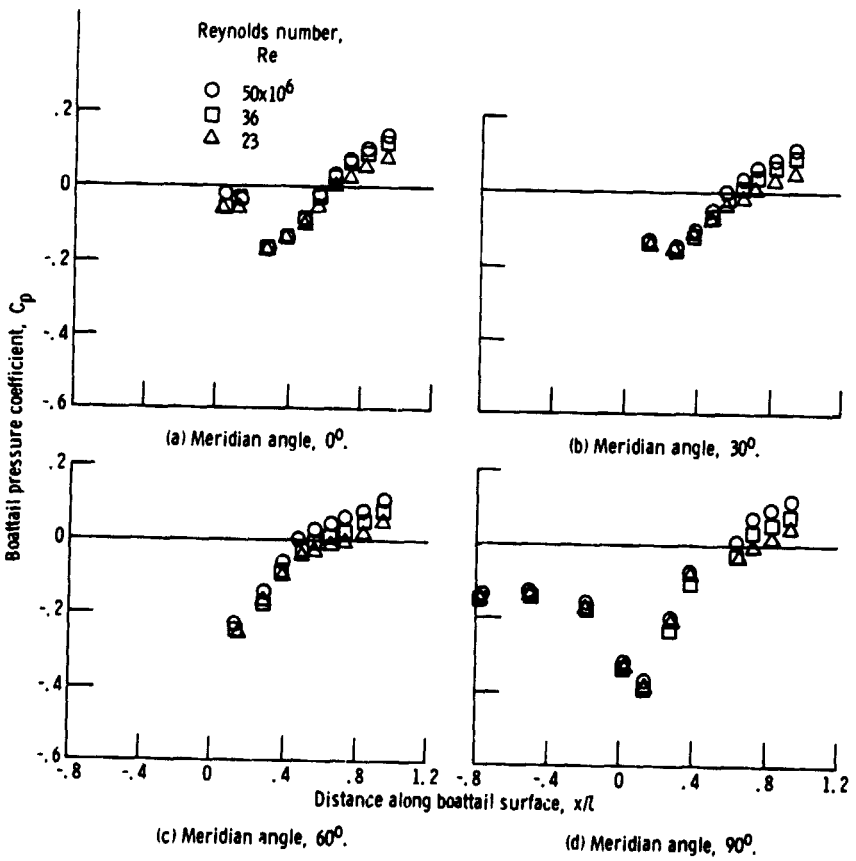

Figure 11. - Effect of Reynolds number on boattail pressure distribution. Mach number, 0.9; angle of attack, 7.5°.

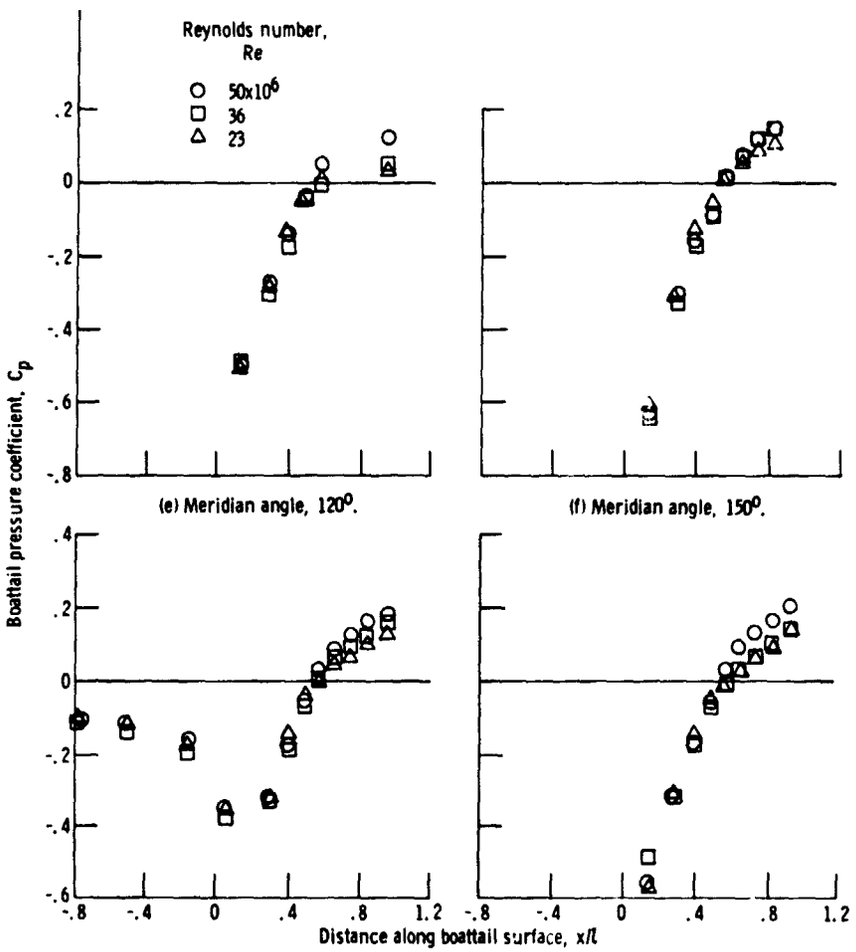

(e) Meridian angle, 120°.

(f) Meridian angle, 150°.

(g) Meridian angle, 180°.

(h) Meridian angle, 210°.

Figure 11. - Continued.

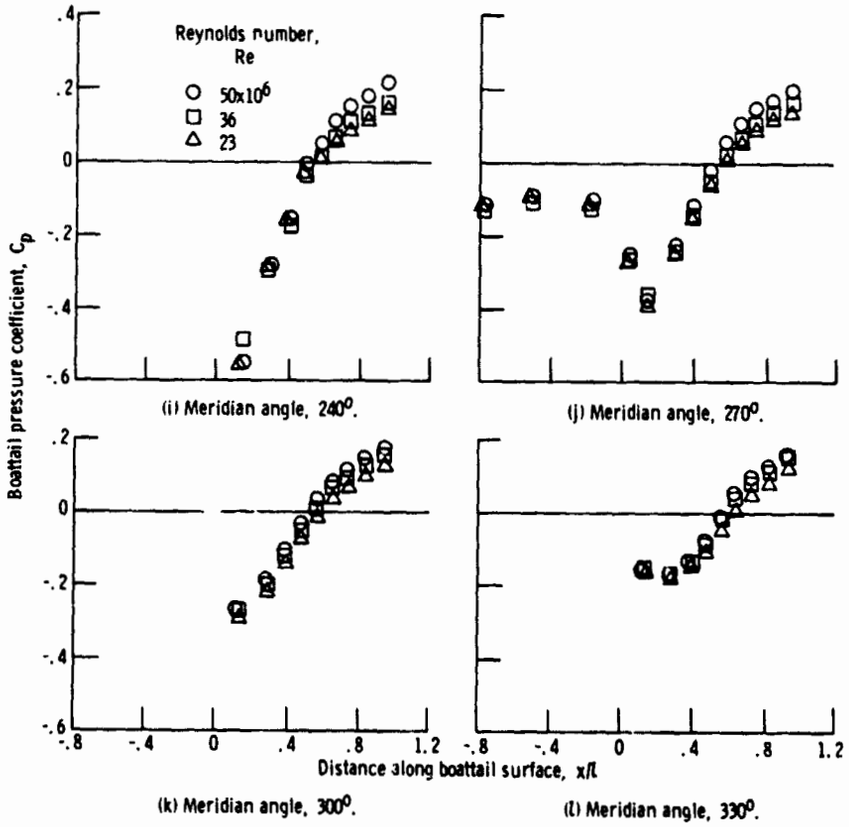

Figure 11. - Concluded.

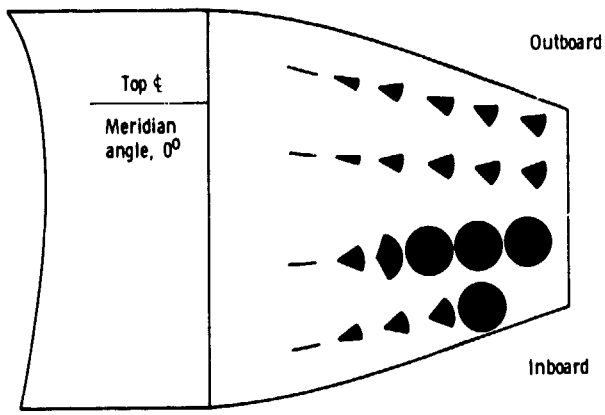

(a) Reynolds number, 50.5×10^6.

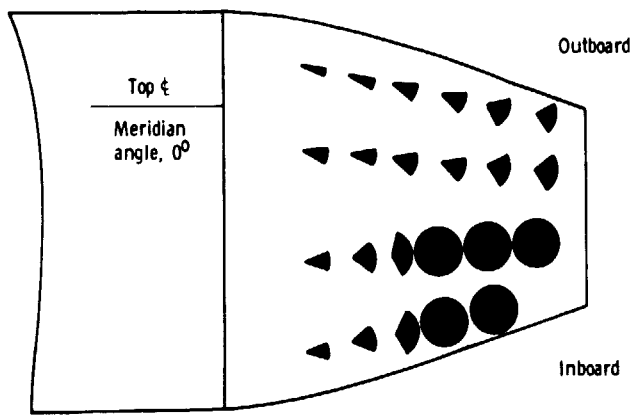

(b) Reynolds number, 22.9×10^6.

Figure 12. - Effect of Reynolds number on amount of tuft movement. Mach number, 0.9; angle of attack, 7.5°. (Shaded areas are areas swept over by tufts.)

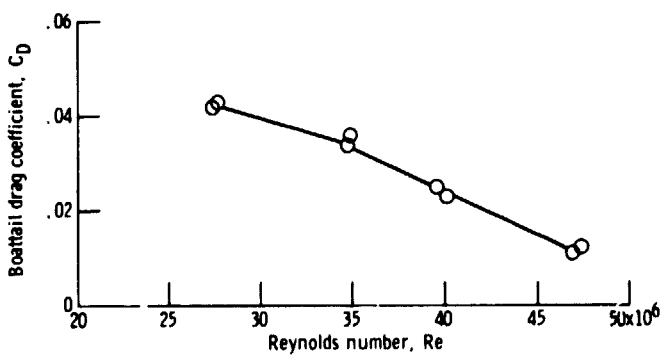

Figure 13. - Reynolds number effect on boattail drag coefficient. Mach number 0.6; angle of attack, 10°.

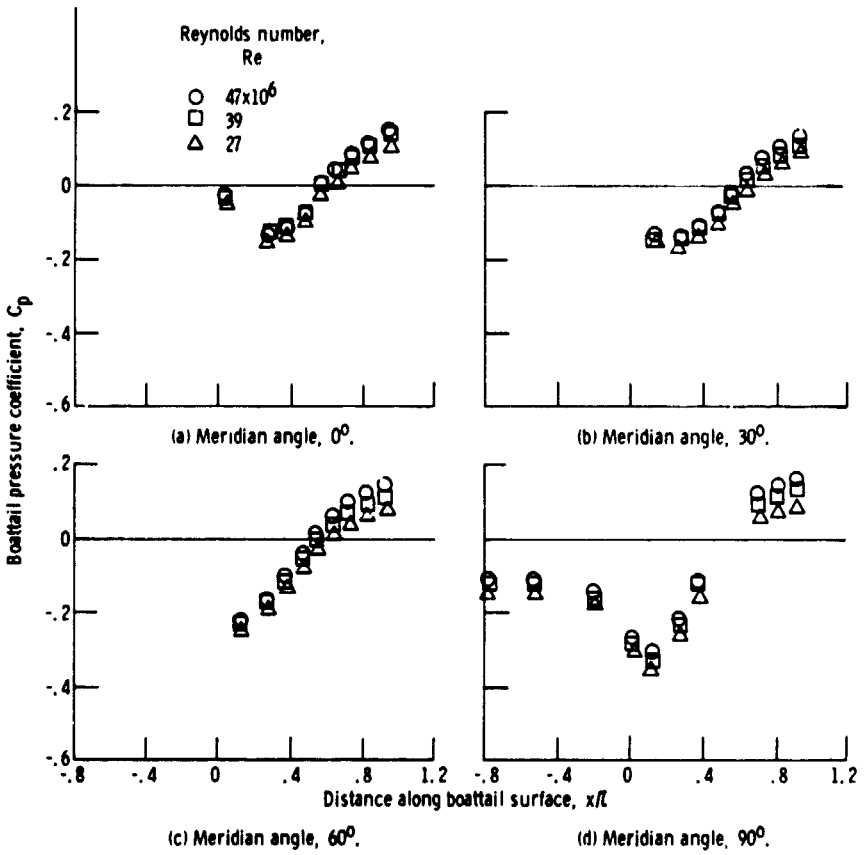

Figure 14. - Effect of Reynolds number on boattail pressure distribution. Mach number, 0.6; angle of attack, 10°.

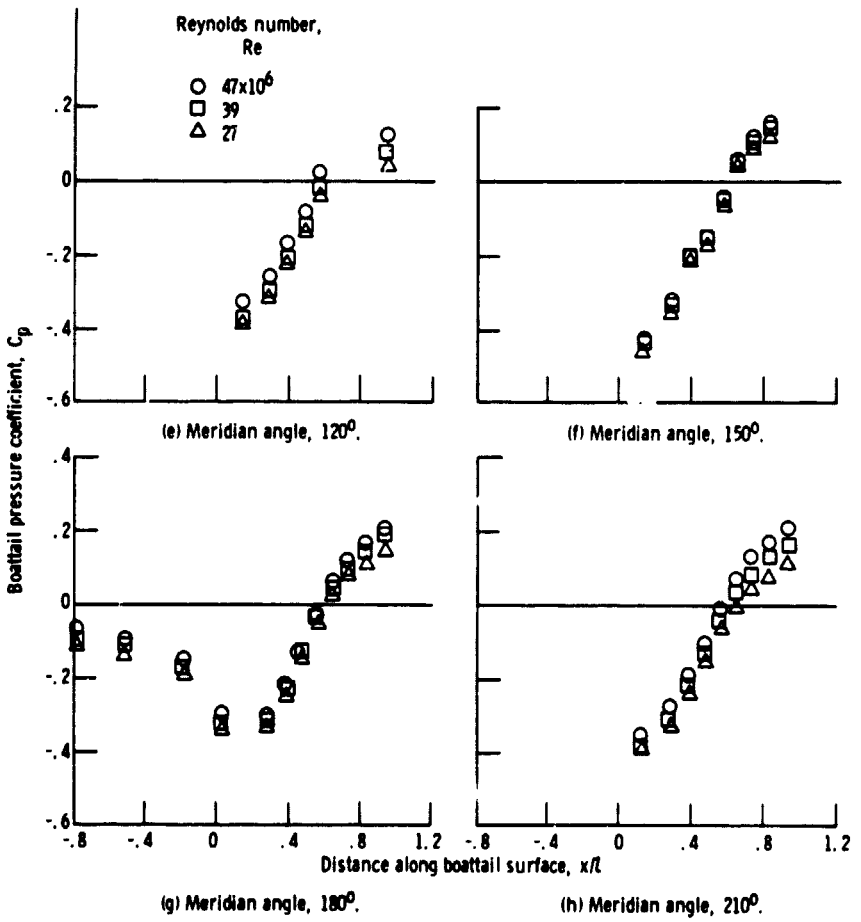

Figure 14. - Continued.

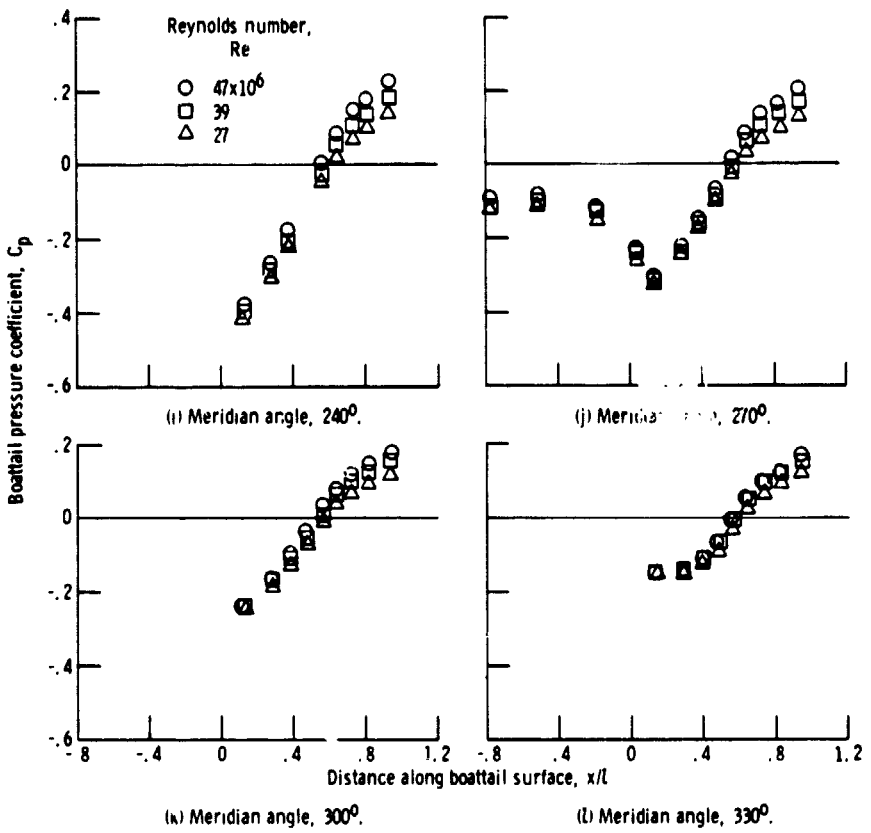

Figure 14. - Concluded.

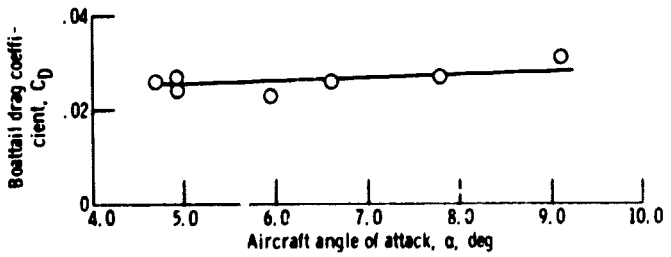

Figure 15. - Angle of attack effects on boattail drag. Mach number, 0.9; Reynolds number, 36.0×10^6; altitude, 10 668 meters (35 000 ft).

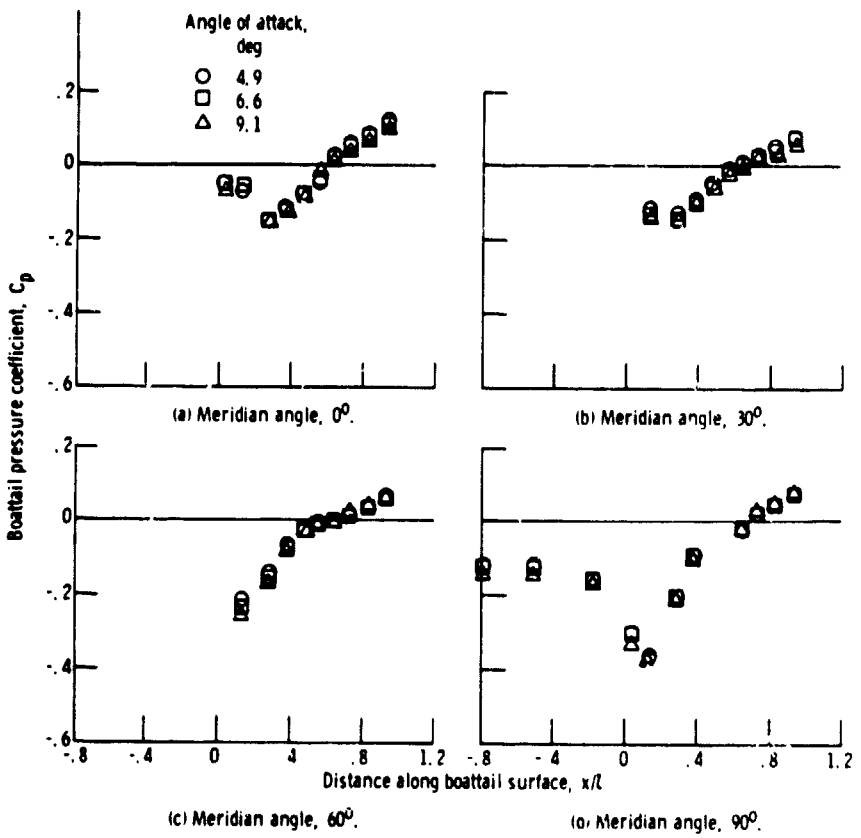

Figure 16. - Effect of angle of attack on boattail pressure distribution. Mach number, 0.9; Reynolds number, 35×10^6.

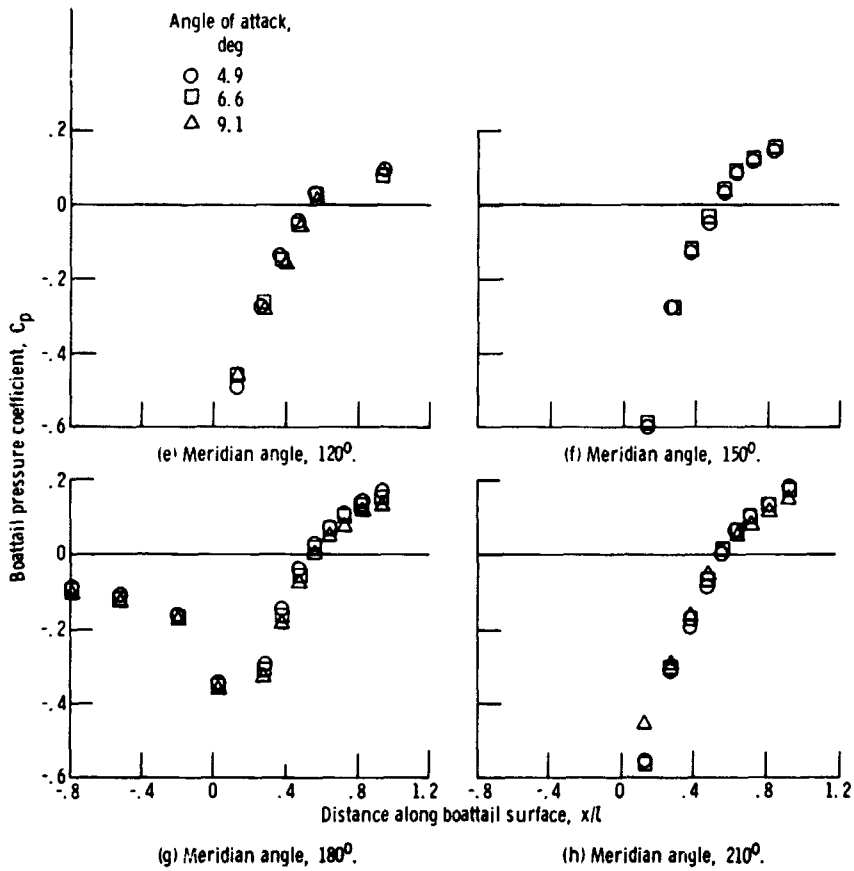

Figure 16. - Continued.

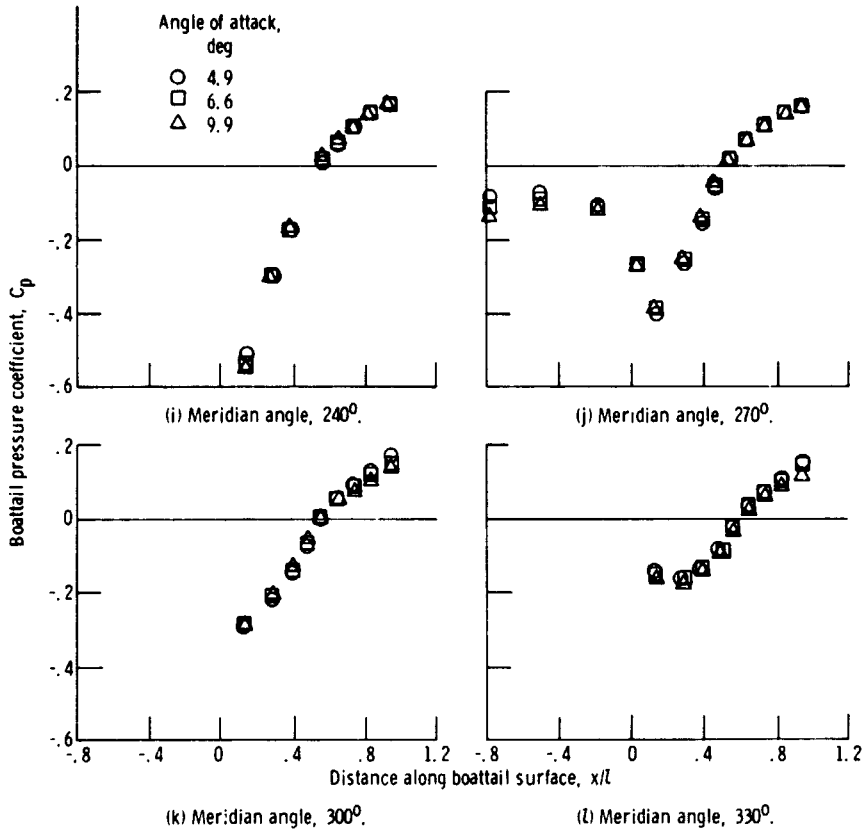

Figure 16. - Concluded.

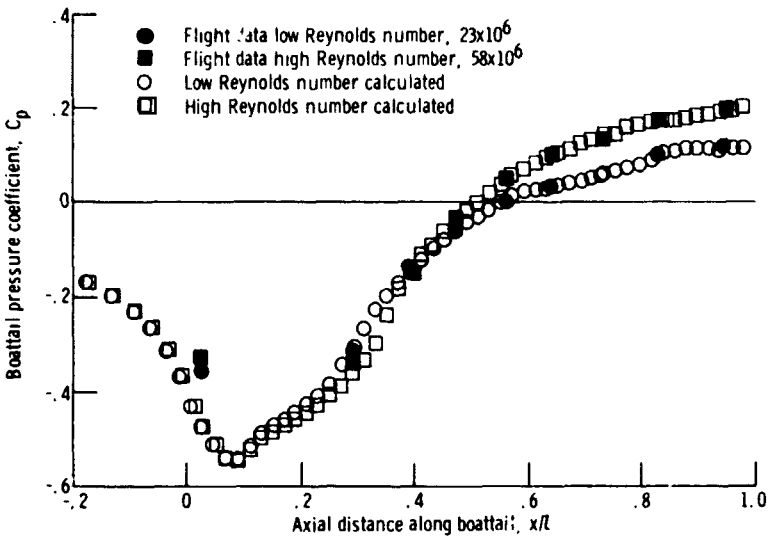

Figure 17. - Comparison of calculated pressure distributions with flight pressures. Mach number, 0.9; flight data measured at 180° meridian angle.

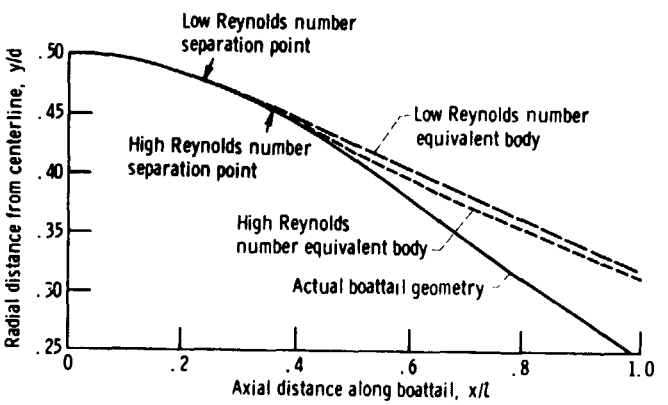

Figure 18. - Equivalent body shapes used for calculation of separated flow pressure distributions. Mach number, 0.9.